PHYSICAL REVIEW B VOLUME 40, NUMBER 9 15 SEPTEMBER 1989-II

Scanning tunneling microscope as a probe of the local transport field in mesoscopic systems

C. S. Chu and R. S. Sorbello
Department of Physics and Laboratory for Surface Studies, University of Wisconsin–Milwaukee, Milwaukee, Wisconsin 53201
(Received 8 May 1989)

A theoretical analysis of the local electric field associated with dc conduction in mesoscopic systems is presented, and the possibility of probing this field with the scanning tunneling microscope (STM) as in the measurements of Kirtley *et al.* is theoretically investigated. The theory is based on a Landauer-type analysis in which a given distribution of electrons is incident upon a disordered mesoscopic system. Results are presented for a thin film containing grain boundaries within the jellium model. In the case of an ultrathin film with only one occupied transverse subband and in the case of a random distribution of parallel grain boundaries modeled as semiclassical barriers, the voltage drop measured by the STM ($\delta V_{\rm STM}$) does equal the voltage drop in the local transport field ($\delta V_{\rm LTF}$) across a grain boundary. In the more general case, $\delta V_{\rm STM}$ does not equal $\delta V_{\rm LTF}$, but they are of the same order of magnitude. It is also found that $\delta V_{\rm STM}$ exhibits larger quantum-size effects than $\delta V_{\rm LTF}$.

When an electron current passes through a conductor that contains defects, a local electric field is set up in the vicinity of each of the defects. As shown by Landauer,[1] the origin of this local transport field (LTF) is the charge pileup of carriers incident upon and scattered by the defect. For a macroscopic system, the total LTF for all the defects results in a macroscopic voltage drop along the sample, and this is the voltage associated with the residual resistivity due to the defects.[1,2] Clearly, a complete description of electron transport in macrosopic or mesoscopic systems requires a correct picture of the LTF. In this regard, a direct experimental measurement of the LTF in the immediate vicinity of an individual defect would be of fundamental value.

Recently, efforts have been made to measure the LTF across a grain boundary in a current-carrying conductor by means of the scanning tunneling microscope (STM).[3–5] In these experiments, the STM tip is held at a fixed distance above the sample surface as the tip is scanned over the sample. The local potential in the sample is then identified with the bias potential between the STM tip and the sample under the condition of zero tunneling current. The experimentally determined STM voltage appears to show a local potential drop in the immediate vicinity of a grain boundary,[4] just as might be qualitatively expected for the LTF on the basis of Landauer's picture.[1,6] The obvious question arises: Does the STM really measure the LTF? We address this question in the present paper.

Although it may seem natural to associate the LTF with the measured STM voltage, one can argue that they can indeed be very different. After all, the LTF is essentially proportional to the local pileup of electron density associated with the electron scattering states,[1,2,7,8] while the STM does not directly measure this electron pileup. Rather, the STM is most sensitive to those electron wave functions that extend farthest outside the surface,[9] and these electron states are not necessarily representative of the total set of electron states involved in the LTF. Thus, we do not expect the STM voltage to measure the LTF. Our detailed analysis for the grain-boundary problem corroborates this view, but we do find two important cases where the STM does measure the LTF. We also find that the STM voltage is often not very different from the LTF for the models investigated here.

We consider a grain boundary in a thin metal film. For a given incident electron distribution, the drop in the LTF across the grain boundary is to be compared with the drop in the measured STM voltage across the grain boundary. The incident electron distribution is taken to be of a general form, with a reservoir-type distribution included as a special case. The problem is a three-probe configuration and the analysis is similar to that of Büttiker[10] except that the third probe is a STM tip, effectively probing only one point on the film surface at one time. The metallic thin film is taken to confine an electron gas by finite potential barriers. The confining potential $U_c(z)$ is given by

$$U_c(z)=\begin{cases}0, & \dfrac{-W}{2}<z<\dfrac{W}{2}\\ U_o, & |z|\geq\dfrac{W}{2}\end{cases} \tag{1}$$

where W is the width of the film. The unperturbed electron states $\psi^0_{n\mathbf{k}}$ in the film have the form

$$\psi^0_{n\mathbf{k}}(\mathbf{r})=\frac{e^{i\mathbf{k}\cdot\boldsymbol{\rho}}}{\sqrt{A}}\phi_n(z)\ , \tag{2}$$

where A is the area of the film, $\mathbf{k}=(k_x,k_y)$, and $\boldsymbol{\rho}=(x,y)$. Here n is the subband index and $\phi_n(z)$ satisfies the equation

$$\left[-\frac{\hbar^2}{2m^*}\frac{\partial^2}{\partial z^2}+U_c(z)\right]\phi_n(z)=E_n\phi_n(z)\ ,$$

where m^* is the effective mass. The energy of the state $\psi^0_{n\mathbf{k}}$ is $E_{n\mathbf{k}}=E_n+\hbar^2k^2/2m^*$. Since we are interested only in the scattering of electrons at the Fermi level E_F, the magnitude of the wave vector k for an occupied subband (n) becomes k_{Fn}. A grain boundary lies parallel to y direction in the film and its potential U_B is modeled as

$$U_B=\begin{cases}0, & x<0 \text{ or } x>\Delta \\ fE_{FB}, & 0<x<\Delta\end{cases}, \tag{3}$$

where Δ is the width of the grain boundary, and the barrier height is expressed in units of E_{FB}, the bulk Fermi energy for a given electron density, with f a dimensionless parameter. In modeling the grain boundary as a potential barrier within the jellium model, we are of course neglecting the details of the lattice structure and the lattice mismatch at the grain boundary. Nonetheless, the model has been shown to be useful,[11] if only very approximate. In writing Eq. (3), we have neglected the z dependence of U_B and this effectively eliminates interchannel scattering. This schould be a good approximation for strong confining potentials, as is the case for metal films.

In the following analysis, we consider the case where the electron transport current is perpendicular to the grain boundary. We describe the incident electron distribution by the channel-dependent quantities $\mu_{L\alpha}$ and $\mu_{R\alpha}$, where α is the channel index defined by $\alpha\equiv(n,k_y)$. The incident electron states in a given channel α on the left-hand side of the grain boundary (the negative-x region) are taken to be occupied up to an energy $\mu_{L\alpha}$, while the incident electron states on the right-hand side of the grain boundary are taken to be occupied up to an energy $\mu_{R\alpha}$. Since we shall assume the linear-response regime throughout, the quantities $\mu_{L\alpha}$ and $\mu_{R\alpha}$ differ only slightly from the chemical potential μ for the equilibrium system, i.e., for the system in the absence of current flow.

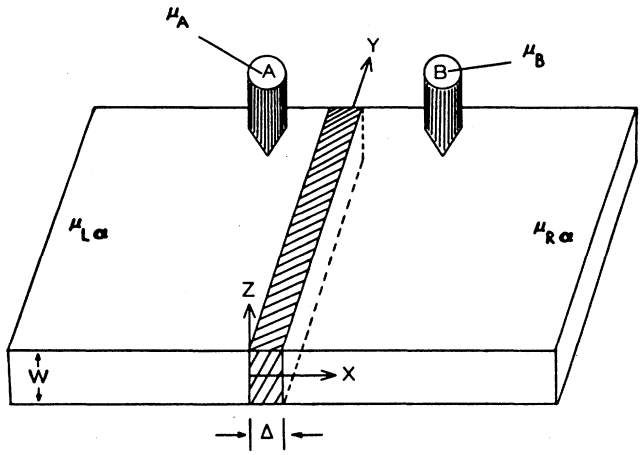

FIG. 1. A schematic diagram of STM measurements in the vicinity of a grain boundary in a metallic film. The transport in the film is set up by an incident electron distribution $\mu_{L\alpha}$ and $\mu_{R\alpha}$ on each side of the grain boundary. The STM tip is placed at location A and then location B. The film thickness is W and the thickness of the grain boundary is Δ.

Now we bring in the STM tip to probe the left-hand region of the grain boundary (see Fig. 1). We assume that the STM tip is only weakly coupled to the electrons in the film so that there is no coherent scattering of the electron between the tip and the film. We also neglect the Friedel oscillations arising from the coherence between the incident electron states and their reflected waves from the grain boundary.[12] For a state $\psi^0_{n\mathbf{k}}$ incident from the left-hand side of the grain boundary $(k_x>0)$, the charge current tunneling into state ν in the STM tip is

$$I_t(n\mathbf{k};\nu)=\frac{2\pi e}{\hbar}[1+R(k_x)]|M(n\mathbf{k};\nu)|^2\delta(E_{n\mathbf{k}}-E_\nu) \quad (k_x>0), \tag{4}$$

where e is the electron charge, $R(k_x)$ is the reflection probability from the grain boundary, and $M(n\mathbf{k};\nu)$ is the tunneling matrix element. For our model potential, the reflection probability $R(k_x)$ is given by

$$R(k_x)=\left|\frac{fk_{FB}^2\sinh(K\Delta)}{2iKk_x\cosh(K\Delta)+(k_x^2-K^2)\sinh(K\Delta)}\right|^2, \tag{5}$$

where $K=(fk_{FB}^2-k_x^2)^{1/2}$, k_{FB} is the bulk Fermi wave vector, and the convention $(-1)^{1/2}=+1$ is implied throughout. For a state $\psi^0_{n\mathbf{k}}$ incident from the right-hand side of the grain boundary $(k_x<0)$, the current tunneling into state ν in the STM tip is given by

$$I_t(n\mathbf{k};\nu)=\frac{2\pi e}{\hbar}T(k_x)|M(n\mathbf{k};\nu)|^2\delta(E_{n\mathbf{k}}-E_\nu) \quad (k_x<0), \tag{6}$$

where $T(k_x)=1-R(k_x)$ is the transmission probability. By symmetry, both $R(k_x)$ and $T(k_x)$ are even functions of k_x.

The tunneling matrix element is of the form[9]

$$|M(n\mathbf{k};\nu)|^2=C_0|\phi_n(z_0)|^2, \tag{7}$$

where C_0 is a constant dependent only on the tip's properties and z_0 is the z component of the position of the STM tip's center of curvature. Expression (7) was derived by Tersoff and Hamann[9] in the spherical-tip approximation in which the wave functions for electrons in the tip are approximated by their s-wave component. We point out that z_0 is outside the film, and so $\phi_n(z_0)$ is the exponential tail of the wave function of subband n in the STM tip region. Thus each occupied subband will contribute differently to the tunneling current, and, in fact, the higher occupied subband, having a longer exponential tail in wave function outside the film, will contribute more.

We now calculate the tunneling current using the general approach of Büttiker.[10] If μ_A is the chemical potential in the STM tip, the total tunneling current I_A into the STM tip is then given by

$$I_A=\sum_{\nu}\sum_{\substack{\alpha k_x \\ (k_x>0)}} I_t(n\mathbf{k};\nu)\delta(E_{n\mathbf{k}}-\mu)(\mu_{L\alpha}-\mu_A)$$

$$-\sum_{\nu}\sum_{\substack{\alpha k_x \\ (k_x<0)}} I_t(n\mathbf{k};\nu)\delta(E_{n\mathbf{k}}-\mu)(\mu_A-\mu_{R\alpha})\ . \tag{8}$$

The first term in Eq. (8) corresponds to the net tunneling current into the STM tip due to excess electrons incident from the left-hand side of the tip. The second term corresponds to the net tunneling current out of the STM tip due to deficit electrons from the right-hand side of the barrier.

By setting $I_A=0$, we can determine the measured μ_A from Eq. (8). The result is

$$\mu_A=\frac{\frac{1}{\pi}\sum_n|\phi_n(z_0)|^2\int_0^{\pi/2}d\theta[R(k_{Fn}\cos\theta)(\mu_{L\alpha}-\mu_{R\alpha})+\mu_{L\alpha}+\mu_{R\alpha}]}{\sum_n|\phi_n(z_o)|^2}\ , \tag{9}$$

where $k_y=k_{Fn}\sin\theta$. The STM tip is now moved to the right-hand side of the grain boundary. The new chemical potential in the STM tip is denoted by μ_B. Following the procedure used in obtaining Eq. (8), we can obtain an expression for the total tunneling current I_B into the STM tip at its new position. Again we set $I_B=0$, and we obtain an expression for μ_B like the right-hand side of Eq. (9) except that L and R are interchanged. It follows that the potential drop (from left to right) across the grain boundary as measured by the STM tip is

$$\delta V_{\rm STM}=\frac{\mu_A-\mu_B}{e}=\frac{2}{\pi e}\frac{\sum_n|\phi_n(z_0)|^2\int_0^{\pi/2}d\theta\,R(k_{Fn}\cos\theta)(\mu_{L\alpha}-\mu_{R\alpha})}{\sum_n|\phi_n(z_0)|^2}\ . \tag{10}$$

In the following, we derive the local transport field drop across a grain boundary in terms of $\mu_{L\alpha}$ and $\mu_{R\alpha}$. The approach closely follows that described by Büttiker *et al.*[13] The incident electron distribution, defined by $\mu_{L\alpha}$ and $\mu_{R\alpha}$, is scattered by the grain boundary and as a result the chemical potential of the electrons becomes $\mu_A(\mu_B)$ on the left- (right-) hand side of the grain boundary. The chemical potential $\mu_A(\mu_B)$ is determined such that the total number of scattered electrons in a given spatial region is equal to the total number of states with energies between $\mu_A(\mu_B)$ and the equilibrium chemical potential μ in the same spatial region.[13] It is simpler to express this condition by reckoning the excess number of electrons with respect to $\mu_{R\alpha}$ rather than μ. Accordingly, on the left-hand side of the grain boundary we have

$$\sum_\alpha\frac{1}{k_{\alpha x}}[1+R(k_{\alpha x})](\mu_{L\alpha}-\mu_{R\alpha})=\sum_\alpha\frac{2}{k_{\alpha x}}(\mu_A-\mu_{R\alpha}), \tag{11}$$

where $k_{\alpha x}$, the effective Fermi wave vector along the x direction for channel α, equals $(k_{Fn}^2-k_y^2)^{1/2}$. The factors $1/k_{\alpha x}$ in the summations come from the density of states. Similarly, on the right-hand side of the grain boundary we have

$$\sum_\alpha\frac{1}{k_{\alpha x}}T(k_{\alpha x})(\mu_{L\alpha}-\mu_{R\alpha})=\sum_\alpha\frac{2}{k_{\alpha x}}(\mu_B-\mu_{R\alpha})\ . \tag{12}$$

The local transport field drop across the grain boundary is then found to be

$$\delta V_{\rm LTF}=\frac{\mu_A-\mu_B}{e}=\frac{2}{\pi e}\frac{\sum_n\int_0^{\pi/2}d\theta\,R(k_{Fn}\cos\theta)(\mu_{L\alpha}-\mu_{R\alpha})}{N}\ , \tag{13}$$

where N is the total number of occupied subbands, and the integral over θ arises from the generalized sum (integration) over k_y. (We have also made use of the even symmetry with respect to k_y.) The potential drop $\delta V_{\rm LTF}$ occurs over distances on the order of a screening length from the grain boundary.[1] (The same is true of $\delta V_{\rm STM}$ for our grain-boundary model.)

By comparing Eqs. (10) and (13), we see that $\delta V_{\rm STM}$ and $\delta V_{\rm LTF}$ are not equal in general. Higher occupied subbands carry greater weight in $\delta V_{\rm STM}$ through the weighting factor $|\phi_n(z_0)|^2$, as we have mentioned earlier. However, there are exceptions. The obvious one is the ultrathin-film case when there is only one occupied subband and consequently $\delta V_{\rm STM}$ does indeed equal $\delta V_{\rm LTF}$. There is another case where $\delta V_{\rm STM}$ equals $\delta V_{\rm LTF}$, and this will be discussed later.

The analysis thus far has not specified the form of $\mu_{L\alpha}$ and $\mu_{R\alpha}$. In the following we consider three different situations and use the corresponding form of $\mu_{L\alpha}$ and $\mu_{R\alpha}$ to calculate $\delta V_{\rm STM}$ and $\delta V_{\rm LTF}$. In the first situation $\mu_{L\alpha}$ and $\mu_{R\alpha}$ are independent of the channel index α. All the incident channels on the left-hand side of the grain boundary now have the same chemical potential, and similarly for the right-hand side of the grain boundary. This situation corresponds to the reservoir case in which the grain boundary is connected through perfect film conductors to two incoherent reservoirs, one on each side of

the grain boundary. If $\Delta\mu$ is the chemical potential difference between the two reservoirs, then we have for this reservoir case

$$\mu_{L\alpha}-\mu_{R\alpha}=\Delta\mu \ . \tag{14}$$

In the second situation, we consider the conducting film on either side of the grain boundary to contain background scatterers which can be characterized by a collision time τ. Supposing that the background τ in the film dominates the scattering, it follows that $\mu_{L\alpha}=\mu+\Delta\mu_\alpha$ and $\mu_{R\alpha}=\mu-\Delta\mu_\alpha$, where

$$\Delta\mu_\alpha=\frac{eE_0\hbar\tau}{m^*}k_{Fn}\cos\theta=(eE_0l)\frac{k_{Fn}}{k_{FB}}\cos\theta \ , \tag{15}$$

and where E_0 is the electric field set up by the background τ, and l is the bulk mean free path. Here $k_{Fn}\cos\theta$ is the effective Fermi wave vector in the x direction for channel α. The form of $\Delta\mu_\alpha$ is the shifted Fermi-sphere distribution. We point out that in the background-τ case the number of incident electrons in the higher subbands is smaller and this will somewhat offset the effect of the weighting factor $|\phi_n(z_0)|^2$ for the higher subband contributions.

The third situation we consider is a random distribution of parallel semiclassical barriers. In this model, coherent multiple scattering between barriers is neglected. We expect that this model is a reasonable first approximation for weak-scattering grain boundaries in the absence of appreciable background scattering.[14] The electron distribution for the transport problem in this system has been considered by Landauer,[1,6] and the corresponding distribution can be written as $\mu_{L\alpha}=\mu+\Delta\mu_\alpha$ and $\mu_{R\alpha}=\mu-\Delta\mu_\alpha$, where $\Delta\mu_\alpha$ is given by

$$\Delta\mu_\alpha=\frac{e\delta V}{2R\,(k_{Fn}\cos\theta)} \ , \tag{16}$$

with δV being the total voltage across the sample divided by the number of barriers. Substituting Eq. (16) into Eqs. (10) and (13), we find

$$\delta V_{\rm STM}=\delta V_{\rm LTF}=\delta V \ .$$

Therefore in the case of a random distribution of parallel semiclassical barriers, $\delta V_{\rm STM}$ does equal $\delta V_{\rm LTF}$.

We now present the results of numerical calculations for the reservoir case and the background-τ case. The film is chosen to be an aluminum film, where $k_{FB}=0.927$ a.u. and $U_0/E_{FB}=1.36$, which we obtain from the work function for aluminum. For the grain boundary we choose $f=0.2$ and $\Delta=4$ a.u. The distance d of the STM tip to the film surface is chosen to be 9.5 a.u. To calculate $\delta V_{\rm STM}$ by Eq. (10) we require the electronic wave function $\phi_n(z_0)$ outside the film. For our confining potential, given in Eq. (1), we find that

$$|\phi_n(z_0)|^2=\begin{cases} e^{-2\beta d}\left[\dfrac{1}{\beta}+\dfrac{W(1+\xi^{-1}\sin\xi)}{2\cos^2(\xi/2)}\right]^{-1} & \text{for odd } n \\ e^{-2\beta d}\left[\dfrac{1}{\beta}+\dfrac{W(1-\xi^{-1}\sin\xi)}{2\sin^2(\xi/2)}\right]^{-1} & \text{for even } n \end{cases} \tag{17}$$

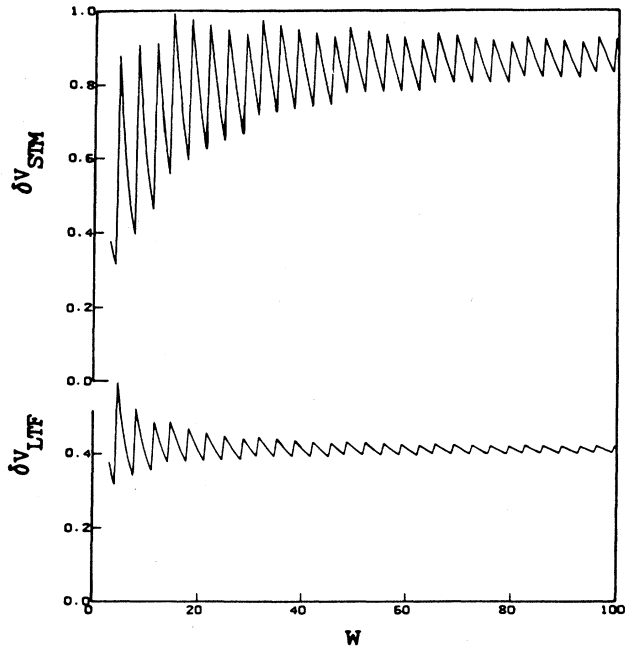

FIG. 2. $\delta V_{\rm STM}$ and $\delta V_{\rm LTF}$ across a grain boundary in an aluminum film plotted as a function of W, the film thickness, for the reservoir case. The vertical axis is in units of $-\Delta\mu$ and the horizontal axis is in atomic units (Bohr radii).

where $d=z_0-W/2$ is the distance of the STM tip from the film surface, $\beta=[2m^*(U_0-E_n)/\hbar^2]^{1/2}$, and $\xi=W(2m^*E_n/\hbar^2)^{1/2}$.

In Fig. 2 we present a plot of $\delta V_{\rm STM}$ and $\delta V_{\rm LTF}$ versus the width W of the film for the reservoir case. Both graphs exhibit sharp oscillations which are attributed to the quantum size effects due to the subband electronic structure in the film. Note that the quantum size effect is larger in the $\delta V_{\rm STM}$ plot. The ratio of $\delta V_{\rm STM}/\delta V_{\rm LTF}$ versus W, as shown in Fig. 3, starts at unity in the ultrathin-film regime and approaches 2.16 in the thick-film limit, which we have obtained by taking $W\gtrsim 2000$

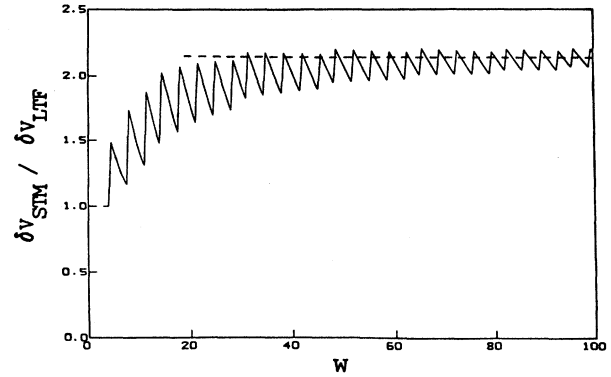

FIG. 3. $\delta V_{\rm STM}/\delta V_{\rm LTF}$ plotted as a function of W for the reservoir case. For large W ($W>2000$ a.u.), the oscillation amplitude is less than 1% of the asymptotic value indicated by the dashed line.

a.u. The oscillations die out gradually as the thickness W is increased. In the thick-film limit when $W \gtrsim 2000$ a.u., the oscillation amplitude is less than 1%. We point out that the upward peaks in the oscillations are associated with the condition that the Fermi surface is at a subband bottom. This is because the highest occupied subband will contribute the most to both δV_{STM} and δV_{LTF} due to large reflection probability from the grain boundary.

In Fig. 4 we present a plot of δV_{STM} and δV_{LTF} versus W for the case of background τ in the film. Quantum size effects can be seen in both graphs with greater oscillations in the δV_{STM} plot. The ratio of $\delta V_{\mathrm{STM}}/\delta V_{\mathrm{LTF}}$ versus W, as shown in Fig. 5 starts at unity in the ultrathin-film regime and approaches 1.2 in the thick-film limit ($W \gtrsim 2000$ a.u.) where the oscillation amplitude is less than 1%. We point out that the downward dips in the oscillations occur when the Fermi surface is very near a subband bottom. This is because at a subband bottom $\Delta\mu_\alpha$ [see Eq. (15)] is zero for the highest subband, and $\Delta\mu_\alpha$ appears in the numerators of Eqs. (10) and (13), while the denominators jump abruptly at a subband bottom.

The quantum-size-effect structure in Figs. 2 and 4 is associated with the discontinuities in the electronic density of states as a function of film thickness. These discontinuities are somewhat smoothed out by departures of the film surface from perfect flatness and by finite-temperature effects. As a first approximation, the long-range irregularities of the film surface are expected to lead to an averaging of the density of states versus W relation over a small window of W values which is on the order of the amplitude of the surface irregularity. This would result in a slight smoothing of the curves in Figs. 2–5 over that window of W values. The underlying oscillations, however, would still persist. Additional smoothing of the curves due to finite-temperature effects can be expected when kT is on the order of the intersubband energy difference around the Fermi level. This implies that at room temperature the oscillations would remain visible for $W \lesssim 100$ a.u.

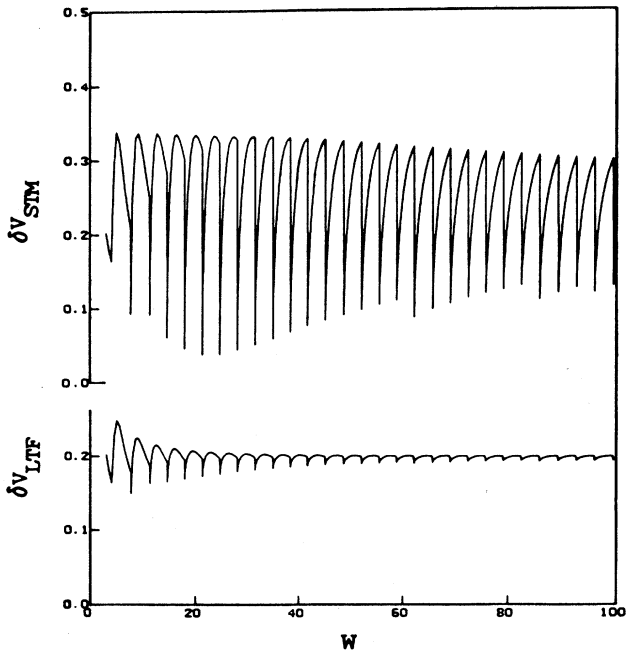

FIG. 4. δV_{STM} and δV_{LTF} across a grain boundary in an aluminum film plotted as functions of W for the case of background τ in the film. The vertical axis is in units of $eE_0 l$ and the horizontal axis is in atomic units.

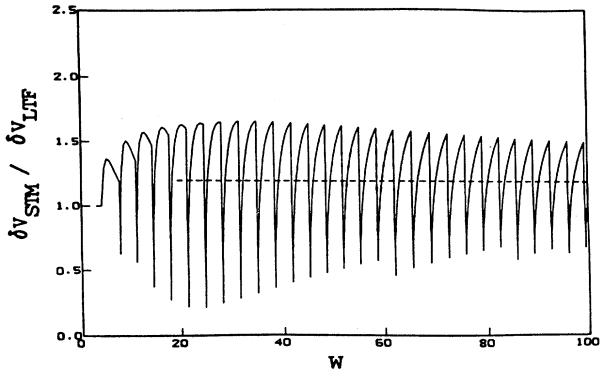

FIG. 5. $\delta V_{\mathrm{STM}}/\delta V_{\mathrm{LTF}}$ plotted as a function of W for the case of background τ in the film. For large W ($W > 2000$ a.u.), the oscillation amplitude is less than 1% of the asymptotic value indicated by the dashed line.

As far as the spatial variation of the local-transport-field voltage V_{LTF} and the local STM voltage V_{STM} is concerned, we point out that both quantities are expected to exhibit similar spatial variation, though in general they are not of equal magnitude. Specifically, beyond a distance on the order of a screening length from a grain boundary, both V_{STM} and V_{LTF} essentially track the local chemical potential, after averaging over a spatial region on the order of a few wavelengths so as to remove the Friedel oscillations common to both V_{LTF} and V_{STM}. The major difference between V_{LTF} and V_{STM} is that V_{LTF} measures the electron probability in all occupied channels, i.e., the local electron density, whereas V_{STM} preferentially weights those occupied channels having large values of transverse momentum (i.e., more rapid oscillations along the z direction within the film). In the case of more general scatterers than the planar grain-boundary model considered here, we can also expect to find evanescent electronic wave functions decaying away from the scatterer. In that case, both V_{LTF} and V_{STM} will pick up the variations occurring within a distance on the order of the electronic-wave-function decay length from the scatterer. However, V_{STM} will show a greater response than V_{LTF} to these wave functions because evanescent waves have larger values of transverse momentum associated with them for a given k_y value.

In conclusion, we find that in general δV_{STM} is not equal to δV_{LTF}, but they are of the same order of magnitude. There are cases where the STM does measure δV_{LTF}, and these are the ultrathin-film case when only one subband is occupied and the case of a random distribution of parallel semiclassical barriers. The fact that

δV_{STM} and δV_{LTF} are of the same order of magnitude is a rather surprising result which allows the STM to probe the LTF, at least qualitatively. We have also found that in the reservoir case and the background-τ case δV_{STM} exhibits larger quantum size effects than δV_{LTF}, and this suggests that the STM can be an effective probe of quantum size effects.

This work was supported by the Rome Air Development Center, United States Air Force.

[1]R. Landauer, IBM J. Res. Dev. **1**, 223 (1957); Z. Phys. B **21**, 247 (1975).
[2]R. S. Sorbello and C. S. Chu, IBM J. Res. Dev. **32**, 58 (1988).
[3]P. Muralt and D. W. Pohl, Appl. Phys. Lett. **48**, 514 (1986).
[4]J. R. Kirtley, S. Washburn, and M. J. Brady, Phys. Rev. Lett. **60**, 1546 (1988).
[5]See also J. R. Kirtley, S. Washburn, and M. J. Brady, Bull. Am. Phys. Soc. **34**, 538 (1989); J. P. Pelz and R. H. Koch, Rev. Sci. Instrum. **60**, 301 (1989).
[6]R. Landauer, in *Electrical Transport and Optical Properties in Inhomogeneous Media,* edited by J. C. Garland and D. B. Tanner (AIP, New York, 1978), p. 2.
[7]R. S. Sorbello, Phys. Rev. B **39**, 4984 (1989).
[8]C. S. Chu and R. S. Sorbello, Phys. Rev. B **38**, 7260 (1988).
[9]J. Tersoff and D. R. Hamann, Phys. Rev. Lett. **50**, 1998 (1983).
[10]M. Büttiker, IBM J. Res. Dev. **32**, 317 (1988).
[11]A. Seeger, Can. J. Phys. **34**, 1219 (1956); J. R. Smith and J. Ferrante, Phys. Rev. B **34**, 2238 (1986).
[12]These Friedel oscillations in the potential can be eliminated from the experimental data by averaging the data over a spatial window on the order of a few Fermi wavelengths.
[13]M. Büttiker, Y. Imry, R. Landauer, and S. Pinhas, Phys. Rev. B **31**, 6207 (1985).
[14]Some incoherent background scattering should be assumed in order to justify the neglect of coherent multiple scattering between grain boundaries that are very far apart. [Of course, if strong incoherent background scattering is assumed, then the background-τ model would be applicable and Eq. (15) holds.]